IEEE Access
Multidisciplinary | Rapid Review | Open Access Journal

Received May 31, 2021, accepted June 15, 2021, date of publication June 18, 2021, date of current version June 29, 2021.

Digital Object Identifier 10.1109/ACCESS.2021.3090396

Model Predictive Control of Soft Constraints for Autonomous Vehicle Major Lane-Changing Behavior With Time Variable Model

FUZHOU ZHAO[1], WENYE WU[1], YANG WU[1], QINGZHANG CHEN[1], YIQUAN SUN[1], AND JIANWEI GONG[2]

[1]School of Automotive Engineering, Changshu Institute of Technology, Suzhou 215500, China
[2]School of Mechanical Engineering, Beijing Institute of Technology, Beijing 100081, China

Corresponding authors: Fuzhou Zhao (zhaofuzhou@cslg.edu.cn) and Jianwei Gong (gongjianwei@bit.edu.cn)

This work was supported in part by the Natural Science Foundation of Zhejiang Province under Grant LY17E050006, and in part by the Ningbo Natural Science Foundation under Grant 2017A610083.

ABSTRACT Changing lane must not only ensure the safety of the vehicle itself, but also ensure the patency of the traffic flow of the original lane and the target lane. Therefore, successful lane-changing is a key technology for autonomous vehicle control. In order to avoid collisions and ensure the smooth flow of traffic, in this paper a vehicle dynamics state model with time variable is established as plant, and the lateral force of the steering wheel is further optimized through Model Predictive Control(MPC), and then the steering wheel angle is obtained to complete the lane-changing operation. The longitudinal and lateral logic controllers designed through soft constraints can better achieve the results of successful lane-changing and unsuccessful return to the original lane, and the lane-changing characteristics within the safety corridor are analyzed in several ways. The simulation analysis of lane-changing strategy at different vehicle velocities provides helpful guidance for the design of autonomous vehicle controllers.

INDEX TERMS Lane-changing, autonomous vehicle, control logic, safety corridor.

I. INTRODUCTION

Since the use of video cameras and Light Detection and Rangings (LIDARs) can better perceive the surrounding traffic conditions and navigate the road ahead through a planned map, autonomous vehicles are gradually entering test roads from the laboratories. Over the past decades, the autonomous vehicles developed in full flourish by various universities and companies worldwide have been bringing a revolution to the automobile industry. Autonomous vehicles have the potential to badly reduce the contribution of driver error and distraction as the cause of vehicle accidents.

The major event in automated vehicle technology was the first Defense Advanced Research Projects Agency (DARPA) Grand Challenge in 2004 and the subsequent DARPA Urban Challenge 2007 [1]. Large numbers of events and major autonomous vehicle system tests have been held. A number of projects have demonstrated higher levels of automation of test vehicles in various research projects [2]. More and more researchers in academia and industry have devoted a lot of efforts to research on improving technologies for autonomous vehicles.

The commercial tests of Google's self-driving vehicles and Tesla's autonomous vehicles have attracted widespread attention from the media and car owners [3]. In addition to traditional automakers such as General Motors (GM) and Bayerische Motoren Werke AG (BMW), many emerging technology companies, such as Apple Inc. (Apple) and Baidu Inc. (Baidu), are also actively following up the research on autonomous technology. Major business's driverless car gave huge publicities to the automated technology and further attracted a pool of talent from several disciplines.

Currently, autonomous driving still faces many technical problems during the course of full commercialization. It is especially worth noting that lane-changing behavior is among the most worthy of research challenge for autonomous driving.

A. LITERATURE REVIEW

Lane-changing maneuvers have profound impacts on the traffic efficiency and the traffic accidents. Parameters of the

The associate editor coordinating the review of this manuscript and approving it for publication was Fangfei Li.

vehicle as the longitudinal velocity, longitudinal acceleration, lateral velocity, lateral acceleration, steering angle, etc. need to be adjusted in real-time when lane-changing [4]. In order to ensure that the self-driving vehicle reliably realizes the lane-changing, vehicle-to-vehicle communication or accurately detecting the traffic flow around the plant can be realized [5]. But not all vehicles have the ability to communicate with the surrounding traffic. For autonomous vehicles, laser radar and millimeter-wave radar can be installed to perceive the safety of the surrounding vehicles. It is difficult for us to reasonably control an autonomous vehicle model with a certain accuracy through its own controller.

J. Funke linearized some governing equations of vehicle states and path states to produce an affine vehicle model, which enables real-time implementation [6]. N. A. Spielberg used a feedforward-feedback control algorithm to control a simple physics-based model of the vehicle to track a path up to the friction limits of the vehicle [7]. J. K. Subosits used the linearized equations of motion to generate linear discrete equations describing the state transitions from one point in space to the next. The discretization points are evenly spaced in time along the nominal trajectory which has the advantage of giving finer spatial resolution in the corners than on straightaways [8]. Whereas almost all those control motion equations are linearized and the autonomous models of vehicle dynamics are a bit simplified.

Additionally, predictive controller can exploit internal model to predict the behavior of the plant, starting at the current time, over a future prediction horizon. Once a future optimal input trajectory has been gotten, only the first element of that trajectory is applied as the input signal to the plant. A receding horizon strategy is used to new output value following the reference trajectory [9], [10]. Jiechao Liu presented a model predictive control-based obstacle avoidance algorithm for autonomous ground vehicles at high speed in unstructured environments. The constraints are only about two vehicle stabilization variables of an obstacle, and the path tracking constraints are not considered [11]. J. Funke linearized the vehicle model at each step around an expected operating point and determined the front tire forces in the MPC optimization [6]. Meng, R. used MPC theory to track the lane change trajectory with the lateral model of constant velocity offset plus sine function [12]. Falcone [13] and Turri [14] unanimously implemented Model Predictive Control (MPC) frameworks that can avoid an obstacle on icy road. Kai Liu [15] utilized MPC algorithm to control the dynamic model of automated vehicles and realized lane-changing maneuver in high-velocity scenarios. However, there is no flexible way to deal with vehicle stability boundary conditions in those literatures. In order to better adapt to changes in vehicle velocity, the constraint weight of the cost function should be appropriately changed.

B. CONTRIBUTION

The contribution of this paper is mainly reflected in two aspects. First, the time-varying state variable control equation is derived from the vehicle dynamics model of the autonomous vehicle. The vehicle dynamics cornering stiffness boundary and lateral position boundary constraints are softened in the optimal MPC cost function following the state discretization equation. The vehicle is temporarily allowed to break through the tire's cornering stiffness and the center line boundary of the road in order to avoid obstacles. Then, the two lane-changing modes respectively with the maximum longitudinal acceleration priority strategy and the minimum longitudinal acceleration priority strategy are compared in typical vehicle velocities, and the causes of lag of the lane changing are analyzed from the perspective that the tire longitudinal and lateral forces are constrained by the tire friction circle.

II. CONTINUOUS PLANT MODELING OF VEHICLE DYNAMICS

Controlling the state of the vehicle by the lateral force of the front wheels can flexibly control the vehicle to reach the planned route as soon as possible. In this way, the error model and motion dynamics equations of the vehicle must be established. In order to facilitate the MPC solution, the continuous model must also be discretized to adapt to iterative calculation.

A. TRACKING ERROR MODEL

The tracking error model is a usually used vehicle motion model in the path tracking control of autonomous vehicles, as shown in Fig. 1. The projection point of the vehicle on the road centerline is S_1, and the radius of curvature of the point S_1 on the road centerline is R. The heading angle of the vehicle is φ, and the course angle at point S_1 is φ_{road}. The heading deviation e_φ, which is positive counterclockwise, represents the angle difference between φ and φ_{road}. The distance deviation e_d in the path tracking process is defined as the distance between the center of the rear axle of the vehicle and its projection point on the centerline of the road, and the distance deviation is defined as positive when the vehicle is on the left side of the centerline. The derivative of the heading deviation of $\dot{e_\varphi}$ is shown in Equation (1). The derivative of the lateral distance deviation of $\dot{e_d}$ is equal to the sum of the two sub-velocities v_x and v_y of the CG projected along the normal direction of the centerline with point S_1, as shown in Equation (2).

$$\dot{e_\varphi} = \dot{\varphi} - \frac{v_x \cos e_\varphi}{R + e_d} = \frac{v_x e_d}{R^2} \tag{1}$$

$$\dot{e_d} = v_x \sin e_\varphi + v_y \cos e_\varphi = v_x e_\varphi + v_y \tag{2}$$

B. VEHICLE STATES

In order to allow the vehicle to track a given desired path quickly and stably, a vehicle-tire model needs to be established to highlight and analyze the vehicle's handling and stability characteristics. The established dynamic model is mainly used as an iteration model of model predictive control, and needs to be simplified based on a more accurate

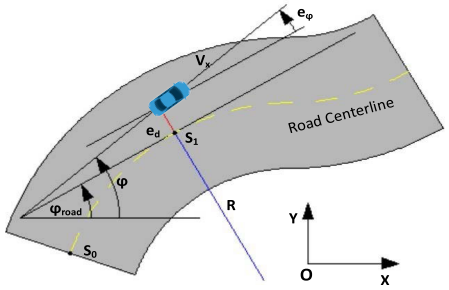

FIGURE 1. Vehicle path tracking model.

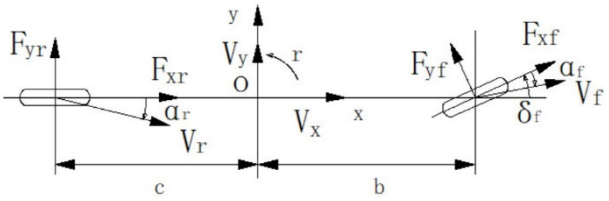

FIGURE 2. Bicycle vehicle dynamics model.

description of the vehicle dynamics process to reduce the computational load of the control algorithm.

This model focuses on the movement of the vehicle along the x-axis and along the y-axis, as well as the rotation around the z-axis, as shown in Fig. 2. The longitudinal force of the center of the front axle is F_{xf}, the lateral force of the center of the front axle is F_{yf}, the velocity of the center of the front axle is $V_{f,}$ the steering angle of the front wheel is δ_f, and the slip angle of the front wheel is α_f. The longitudinal force of the center of the rear axle is F_{xr}, the lateral force of the center of the rear axle is F_{yr}, the velocity of the center of the rear axle is $V_{r,}$ and the slip angle of the rear axle is α_r. The vehicle has an angular velocity of r around the center of gravity (CG). The longitudinal velocity of CG of the vehicle is v_x, the lateral velocity of CG of the vehicle is v_y. The distance from CG of the vehicle to the front axle is equal to b, and that to the rear axle is equal to c.

According to the vehicle force balance and moment balance conditions, the following equations (3) and (4) can be obtained from the dynamics analysis.

$$m\left(\dot{v}_y + v_x r\right) = F_{xf}\sin\delta_f + F_{yf}\cos\delta_f + F_{yr} \tag{3}$$

$$I_z\dot{r} = b\left(F_{xf}\sin\delta_f + F_{yf}\cos\delta_f\right) - cF_{yr} \tag{4}$$

The rear tire will have the velocity component of the CG of v_y along the y-axis and another rotational velocity component of -cr around the CG. The side-slip angle for the rear tire can be expressed as Equation (5). The relationship of linear tire model between the lateral force of the rear wheel of F_{yr} and the slip angle of the rear tire of α_r can be expressed as Equation (6).

$$\alpha_r = \frac{v_y - cr}{v_x} \tag{5}$$

$$F_{yr} = -C_{\alpha r}\alpha_r \tag{6}$$

Combining the above formulas (1), (2), (3), (4), (5) and (6), the resulting vehicle model can be expressed as a continuous form of state space, as shown in formulas (7) and (8). The resulting vehicle model is time-varying, and the radius of curvature of the road centerline of R in the coefficient matrix can be expressed as formula (9) in which δ_f can be obtained by the steering angle in the last iteration calculation.

$$\dot{\xi(t)} = A\xi(t) + Bu(t) \tag{7}$$

$$u(t) = F_{yf}(t) \tag{8}$$

$$R = \frac{57.3L}{\delta_f} \tag{9}$$

$$\text{where} A = \begin{bmatrix} -\frac{C_{\alpha r}}{mv_x} & \frac{cC_{\alpha r}}{mv_x} - v_x & 0 & 0 \\ \frac{cC_{\alpha r}}{I_z v_x} & -\frac{c^2 C_{\alpha r}}{I_z v_x} & 0 & 0 \\ 0 & 0 & 0 & \frac{v_x}{R^2} \\ 1 & 0 & v_x & 0 \end{bmatrix}, \text{ and } B = \begin{bmatrix} \frac{1}{m} \\ \frac{b}{I_z} \\ 0 \\ 0 \end{bmatrix},$$

$$\xi(t) = \begin{bmatrix} v_y & r & e_\varphi & e_d \end{bmatrix}^T$$

The longitudinal displacement d and longitudinal velocity v_x of the vehicle satisfy typical double integrator models. Let the vector ψ represent the composition of two component vectors, then the continuous model can be expressed as Equation (10).

$$\dot{\psi} = \begin{bmatrix} 0 & 1 \\ 0 & 0 \end{bmatrix}\psi + \begin{bmatrix} 0 \\ 1 \end{bmatrix} u_l \tag{10}$$

where $\psi = [d, v_x]^T$ and $u_l = a_x$

III. PLANT MODEL DISCRETIZATION

When using predictive control to iteratively calculate the vehicle model to find the optimal solution of the control variable, the continuous control model equation must be discretized.

For periodic sampling with period T, the model of (7) at some sampling time $t_k = k\cdot T$ can be discretized to differential equations of zero-order holder or first-order holder. It is necessary to consider in detail the tracking error of the trajectory in a short distance, as well as the obstacle situation in a longer distance for self-driving vehicles. In order to reduce the calculation load of the model predictive controller, a variable receding horizon can be used to balance the calculation accuracy and the calculation load. The control horizon N_p is comprised of short prediction horizon N_s and long prediction horizon N_l, as shown in formula (11). In the prediction horizon N_s of the former stage, the sampling period can use a shorter time interval T_s. In the prediction horizon N_l of the later stage, the sampling period can use a longer time interval T_l.

$$N_p = N_s + N_l \tag{11}$$

According to the zero-order holder method, the continuous state differential equation (7) is discretized in the short prediction horizon N_s to obtain the discrete state differential equation (12).

$$\xi(k+1) = A_{ds}\xi(k) + B_{ds}u(k) \tag{12}$$

where $A_{ds} = I_4 + T_s A$ and $B_{ds} = T_s B$

In order to discretize the differential equation with a first-order holder, the auxiliary differential equation (13) is constructed. According to the first-order holder method, the continuous state differential equation (7) is discretized in the long prediction horizon N_l to obtain the discrete state differential equation (14).

$$\begin{bmatrix} \dot{\xi(t)} \\ \dot{u(t)} \\ T_l\ddot{u}(t) \end{bmatrix} = \begin{bmatrix} A & B & 0 \\ 0 & 0 & \frac{1}{T_l} \\ 0 & 0 & 0 \end{bmatrix} \begin{bmatrix} \xi(t) \\ u(t) \\ T_l\dot{u}(t) \end{bmatrix} \tag{13}$$

$$\xi(k+1) = A_{dl}\xi(k) + B_{dl}u(k) + C_{dl}u(k+1) \tag{14}$$

where $A_{dl} = I_4 + AT_l + \frac{1}{2}A^2T_l^2 + \frac{1}{6}A^3T_l^3$

and $B_{dl} = (BT_l + \frac{1}{2}ABT_l^2 + \frac{1}{6}A^2BT_l^3) - (\frac{1}{2}BT_l + \frac{1}{6}ABT_l^2)$

and $C_{dl} = \frac{1}{2}BT_l + \frac{1}{6}ABT_l^2$

In the sampling period T, the relationship between the longitudinal travel distance and the longitudinal velocity of the vehicle with respect to the longitudinal acceleration can also be written as a discrete state equation. As a discretization method of linear interpolation, the first order holder can guarantee a smaller numerical error when the sampling interval T is longer.

Using a first-order holder with the sampling period T, Sampling the double integrator continuous model (10) gives the discrete-time longitudinal system, as shown in formula (15).

$$\psi(k+1) = \begin{bmatrix} 1 & T \\ 0 & 1 \end{bmatrix} \psi(k) + \begin{bmatrix} \frac{1}{2}T^2 \\ T \end{bmatrix} u_l(\mathrm{k}) \tag{15}$$

where $\psi(\mathrm{k}) = [\mathrm{d(k)}, v_x(\mathrm{k})]\mathrm{T}$

and $u_l(\mathrm{k}) = a_x(\mathrm{k})$

IV. LANE-CHANGING CONTROL LOGIC

In this paper, we assume that the autonomous vehicle is trying to change lanes on a two-lane road. Here the target autonomous vehicle is denoted as VB. The nearest vehicle in front of the traffic flow in the original lane is denoted as V1, and the nearest vehicle behind the traffic flow of the original lane is denoted as V3. And the nearest vehicle in front of the traffic flow in the target lane is denoted as V2, and the nearest vehicle behind the traffic flow in the target lane is denoted as V4. The relative positional relationship of these five vehicles is shown in Fig. 3. The lane changing process can be made up of three stages - Traveling in its own lane, Trans-traveling in two lanes, and Traveling in the target lane.

When the vehicle VB is traveling in its own lane with the first phase of lane change, longitudinal control is required to adjust the velocity and displacement of the vehicle VB in order to adapt the traffic flow composed of VB, V1 and V3, and to determine the prediction horizon to start the lane changing. When the vehicle VB is trans-traveling across two lanes with the second phase of lane changing, it requires longitudinal control to adjust the velocity and displacement

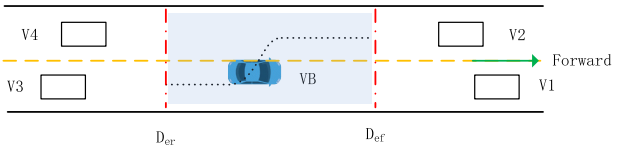

FIGURE 3. Relative positional relationship of five vehicles.

of the vehicle VB, and lateral control of the velocity and displacement of the vehicle VB in order to adapt the traffic flow composed of VB, V1, V3, V2, and V4. When the vehicle VB is traveling in the target lane with the third phase of lane change, it needs to be controlled again longitudinally to adjust the velocity and displacement to adapt the traffic flow composed of VB, V2 and V4, and finally completes the lane changing process. The three stages of lane changing consist of longitudinal control logic and lateral control logic as below.

A. LONGITUDINAL CONTROL LOGIC

First, the lane changing time period T_p is divided into N_p prediction horizons, then each prediction horizon, such as the kth prediction horizon, is examined in detail. When $k \leq N_p$, the maximum longitudinal distance D_{bmax} can be obtained according to the maximum longitudinal acceleration a_{xmax}. According to the minimum longitudinal acceleration a_{xmin}, the minimum longitudinal distance D_{bmin} can also be gotten. The nearest traffic flow distance of the front traffic flow in its own lane as the maximum actual distance D_{ft} can be gotten, and the nearest traffic flow distance of the rear traffic flow in its own lane as the minimum actual distance D_{rt} can also be gotten. According to the formula (17), we can get the length of the safe driving longitudinal corridor of P that the autonomous vehicle can travel. If $P \leq 0$, delay one sampling period and continue to search for future optimal time of lane changing. If $P > 0$ and $K_{gap} < Gap_{min}$, renew the values of K_{start} and K_{end}, and set $K_{gap} = K_{end} - K_{start}$, and then scroll forward one prediction horizon. If $P > 0$ and $K_{gap} \geq Gap_{min}$, then find out the sampling time of the lane changing. This control logic can be shown in Fig. 4.

The maximum actual distance D_{ft} of the forward traffic flow is equal to the nearest calculated distance of the forward traffic flow of D_{ftmin} minus the vehicle body margin D_{margin}, as shown in formula (16a). The minimum actual distance $D_{rt}$of the rear traffic flow is equal to the nearest calculated distance of the rear traffic flow of D_{rtmax} plus the vehicle body margin D_{margin}, as shown in formula (16b). Taking the minimum value of the maximum actual distance D_{ft} and the maximum longitudinal distance D_{bmax} of the forward traffic flow can obtain the forward safety distance Def, as shown in formula (16c). Taking the maximum value of the minimum actual distance D_{rt} and the minimum longitudinal distance D_{bmin} of the rear traffic flow can obtain the rear safety distance D_{er}, as shown in formula (16d). Therefore, the length of the safe driving longitudinal corridor of P in the lane changing

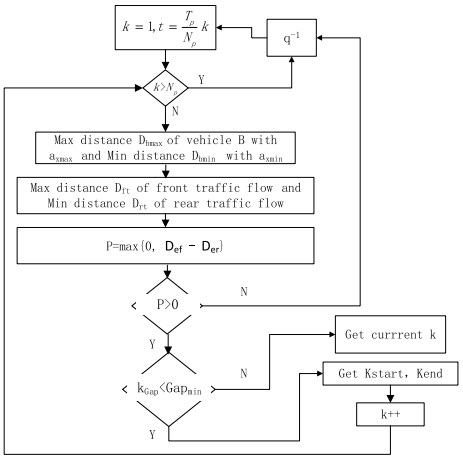

FIGURE 4. Schematic of adjusting the state in one lane.

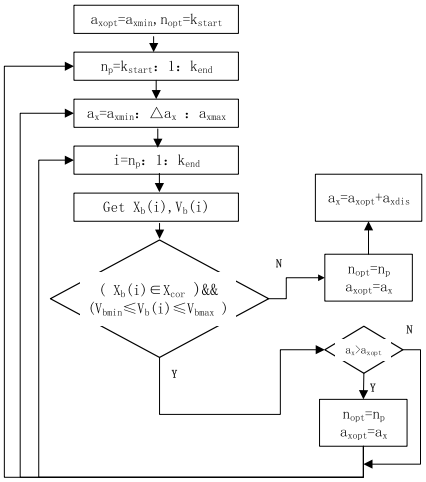

FIGURE 5. Schematic of maximum acceleration strategy.

can be expressed by formula (17).

$$D_{ft} = D_{ftmin} - D_{margin} \tag{16a}$$
$$D_{rt} = D_{rtmax} + D_{margin} \tag{16b}$$
$$D_{ef} = \min\{D_{ft}, D_{bmax}\} \tag{16c}$$
$$D_{er} = \max\{D_{rt}, D_{bmin}\} \tag{16d}$$
$$P = \min\{0, D_{ef} - D_{er}\} \tag{17}$$

B. LATERL CONTROL LOGIC

If a suitable lane changing time is found in the prediction horizon N_p, the longitudinal acceleration of the lane changing can be calculated. When changing lanes, we can select an acceleration value within the allowable range of longitudinal acceleration a_x to change lanes. In this paper, two acceleration lane changing strategies are selected, lane-changing with the maximum acceleration strategy, as shown in Fig. 5, and lane-changing with the minimum acceleration absolute value strategy, as shown in Fig. 6.

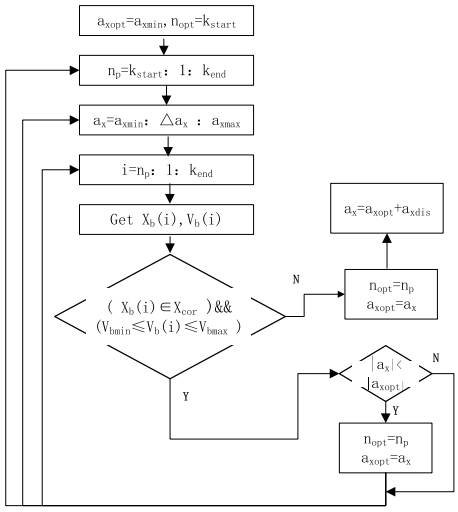

FIGURE 6. Schematic of minimum acceleration absolute value strategy.

1) LANE-CHANGING WITH THE MAXIMUM ACCELERATION STRATEGY

After figuring out the occasion of lane change, from the starting point K_{start} of prediction horizon to the ending point K_{end} of that, the longitudinal displacement $X_{b(i)}$ and the longitudinal velocity $V_{B(i)}$ of the autonomous vehicle are calculated one by one. If the value of $X_{b(i)}$ is within the range of the longitudinal corridor X_{cor},and the longitudinal velocity $V_{B(i)}$ is within the range of the velocity limit, the larger value of acceleration is selected as the acceleration for preferential lane change. If the $X_{b(i)}$ value exceeds the range of the longitudinal corridor X_{cor},or the longitudinal velocity $V_{b(i)}$ exceeds the velocity limit range, the prediction horizon N_p is the optimal lane change prediction horizon N_{opt}, and the longitudinal acceleration a_x is the optimal initial longitudinal Acceleration a_{xopt}. The acceleration a_{xopt} plus the dissipation longitudinal acceleration a_{xdis} equals the optimal longitudinal acceleration a_x. The formula for dissipating longitudinal acceleration a_{xdis} is shown in equation (18), which consists of the dissipating acceleration of drag and that of rolling resistance.

$$a_{xdis} = \frac{\rho V^2 C_D A}{2m} + f_r g \tag{18}$$

2) LANE-CHANGING WITH THE MINIMUM ACCELERATION ABSOLUTE VALUE STRATEGY

If the value of $X_{b(i)}$ is within the range of the longitudinal corridor X_{cor} and the longitudinal velocity $V_{b(i)}$ is within the range of the velocity limit, the smaller value of the absolute value of the acceleration is selected as the priority for the acceleration of the lane change. The other control steps are the same as in the maximum acceleration strategy.

Another important lateral control logic is the front wheel angle control, shown as in Fig. 7. First, the current position of the autonomous vehicle is identified, and the current state

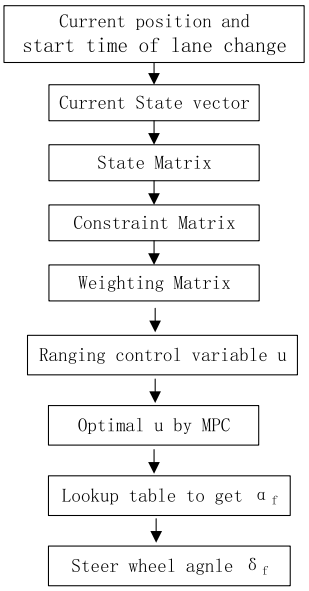

FIGURE 7. Schematic of front wheel steering angle control.

variable vector $\xi(t) = \left[\, v_y \;\; r \;\; e_\varphi \;\; e_d \,\right]^T$ is calculated from the current position, the start position of the lane changing and the target lane centerline. Next, the coefficient matrix of the discrete differential equation of A_{ds}, B_{ds}, A_{dl}, B_{dl}, C_{dl} are gotten, the coefficient matrix of the constraint equation of A_{lp}, B_{lp}, A_{cs}, B_{cs} are also calculated, the weight matrix are figured out. Then the limit range of the control variable u, i.e., F_{yfopt}, from the tire friction ellipse are obtained, and the front wheel slip angle α_f can be found out by the look-up table. Finally, the front wheel steering angle δ_f is calculated by formula (26), and the vehicle VB travels at this front wheel steering angle δ_f for the next sampling period.

The different acceleration control strategies from Fig. 5 and Fig. 6 can obtain the optimal calculated longitudinal acceleration a_{xopt}, and then add the dissipation acceleration a_{xdis} defined by formula (18) to obtain the actual optimal longitudinal acceleration of a_x [16]. Furthermore, the actual optimal longitudinal force of the front wheel of F_{xf} can be obtained by formula (19). Fig. 8 shows the characteristics of the front tire force friction ellipse. This characteristic can be quantitatively described by formula (20), and thus the allowable range of the front wheel longitudinal force of F_{xf} can be obtained.

$$F_{xf} = \frac{c}{l} m a_x \tag{19}$$

$$\frac{(F_{xf})^2}{(k_{sur}\mu F_{zf})^2} + \frac{(F_{yf})^2}{\left(\frac{k_{sur}\mu F_{zf}}{\eta}\right)^2} A \le 1 (\eta \ge 1) \tag{20}$$

Autonomous vehicle VB needs to be restricted by the position of the centerline of the left or right lanes when lane changing. This constraint condition, shown as in inequality (21), can be further used as a soft constraint for MPC. In order to avoid collisions and change lanes swiftly, it is possible to slightly break this constraint condition.

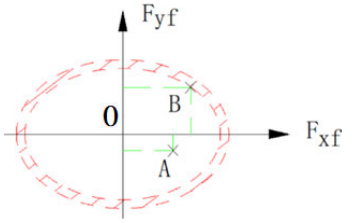

FIGURE 8. Friction ellipse model of front tires.

Lateral position constraints:

$$A_{lp}\xi(k) \le B_{lp}(k)$$

$$A_{lp} = \begin{bmatrix} 0 & 0 & 0 & 1 \\ 0 & 0 & 0 & -1 \end{bmatrix}, B_{lp} = \begin{bmatrix} e_{ymax}(k) \\ -e_{ymin}(k) \end{bmatrix} \tag{21}$$

To prevent sideslip, the side slip angle of the rear wheel of the autonomous vehicle needs to be maintained within a certain limited value range during lane changing. This constraint condition is shown as in inequality (22). In addition, to avoid a sharp spin, the yaw rate of the self-driving vehicle needs to be restricted, and the restriction conditions are shown as in inequality (23). Combining constraint inequality conditions (22) and (23) forms a new constraint inequality (24).

$$-\alpha_{rlim} \le \frac{v_y - cr}{v_x} \le -\alpha_{rlim} \tag{22}$$

$$-r_{lim} \le r \le r_{lim} \tag{23}$$

$$-B_{cs}(k) \le A_{cs}\xi(k) \le B_{cs}(k)$$

$$A_{cs} = \begin{bmatrix} \frac{1}{V_x(k)} & -\frac{c}{V_x(k)} & 0 & 0 \\ 0 & 1 & 0 & 0 \end{bmatrix},$$

$$B_{cs} = \begin{bmatrix} \alpha_{rlim}(k) \\ r_{lim}(k) \end{bmatrix} \tag{24}$$

Instead of weighting control variable u=F_{yf} to reduce the maximum steering angle, MPC optimization weights the state variable $\xi(k)$ and the change of control variable $u = F_{yf}^k - F_{yf}^{k-1}$ to reduce lateral motion acceleration, and weights the soft constraints of the conditions as well to temporarily break through the vehicle stability conditions. The final MPC optimization takes the following form.

$$\begin{aligned} MinimizeJ = {} & \lambda \sum_{k=1}^{Ns} \|\xi(k)\|^2_{Q(k)} + \sum_{k=Ns+1}^{Np} \|\xi(k)\|^2_{Q(k)} \\ & + \lambda \|(u(0) - u_m)\|^2_{R(k)} + \lambda \sum_{k=1}^{Ns} \|(u(k) - u(k-1))\|^2_{R(k)} \\ & + \sum_{k=Ns+1}^{Np} \|(u(k) - u(k-1))\|^2_{R(k)} + \lambda \sum_{k=1}^{Ns} \|S_{cs}(k)\|^2_{T(k)} \\ & + \sum_{k=Ns+1}^{Np} \|S_{cs}(k)\|^2_{T(k)} + \sum_{k=1}^{Ns} \|S_{lp}(k)\|^2_{W(k)} \end{aligned} \tag{25}$$

s.t.

$$\xi(k+1) = A_{ds}\xi(k) + B_{ds}u(k), \forall k = 0, 1, \ldots, Ns-1 \quad (25a)$$

$$\xi(k+1) = A_{dl}\xi(k) + B_{dl}u(k) + C_{dl}u(k+1), \forall k = Ns, Ns+1, \ldots, Np \quad (25b)$$

$$|u(k)| \leq F_y max, \forall k = 0, 1, \ldots, Np-1 \quad (25c)$$

$$-B_{cs}(k) - S_{cs}(k) \leq A_{cs}\xi(k) \leq B_{cs}(k) + S_{cs}(k), \forall k = 1, 2, \ldots, Np \quad (25d)$$

$$S_{cs}(k) \leq S_{csmax}, \forall k = 1, 2, \ldots, Np \quad (25e)$$

$$A_{lp}\xi(k) \leq B_{lp}(k) + S_{lp}(k), \forall k = 1, 2, \ldots, Ns \quad (25f)$$

$$S_{lp}(k) \leq S_{lpmax}, \forall k = 1, 2, \ldots, Ns \quad (25g)$$

The slack variables $S_{cs}(k)$ is added to inequality (24) to become inequality (25d) with one MPC soft constraint condition, and the slack variables $S_{lp}(k)$ is added to inequality (21) to become inequality (25f) with another MPC soft constraint condition. The soft restraints allow the tire force to enter a slightly non-linear state.

The optimal front wheel lateral force F_{yf} is obtained through MPC optimization, and then the side slip angle α_f of the front tire can be obtained by the tabular look-up method, and finally the front wheel streering angle δ_f can be obtained by formula (26).

$$\delta_f = (\beta + \frac{br}{v_x} - \alpha_f)\frac{\pi}{180} \quad (26)$$

V. SIMULATION RESULTS AND DISCUSSIONS

1) The three successful lane-changing path planning profiles shown in Fig. 9 are obtained with the initial vehicle velocities and positions of the three traffic flows defined in Table 1, and also the three unsuccessful lane-changing path planning profiles shown in Fig. 10 with the initial vehicle velocities and positions of the other three traffic flows defined in Table 2.

Under high-velocity, medium- velocity and low- velocity conditions, the minimum acceleration a_{xmin} priority strategy can successfully achieve lane changing and collision avoidance. When changing lanes, it is possible to calculate in real time the safety distance among vehicle VB and the vehicle V1 in front of the lane, the vehicle V3 behind the lane, the vehicle V2 in front of the target lane, and the vehicle V4 behind the target lane in this process. In the prediction horizon, under the conditions that the VB maintains a safety corridor from the front and rear vehicles and remains the acceleration range constraints, the vehicle VB keeps changing lanes according to the smallest possible forward acceleration. When changing lanes according to the minimum acceleration a_{xmin} strategy, both high-velocity lane change and low-velocity lane change can be completed within 5∼13 seconds, but the high-velocity lane changing presents a large overshoot control characteristic in the prediction horizon and the oscillation is obvious. Low-velocity lane change exhibits under-damped control characteristics. The displacement characteristics of successful lane-changing are shown in Fig. 9. In the case of unsuccessful lane-changing, the vehicle VB also has increased oscillation at high velocity when

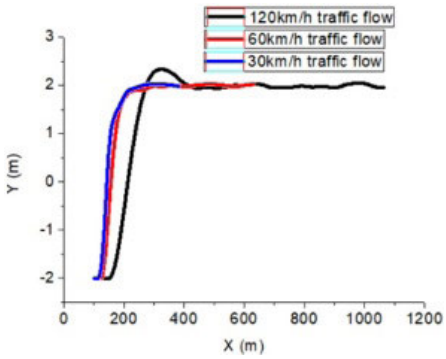

FIGURE 9. Successful lane-changing with scenario a), scenario b), scenario c).

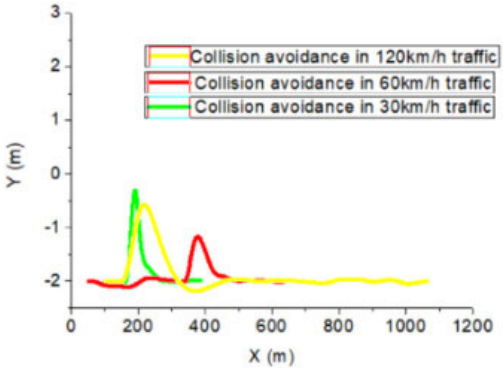

FIGURE 10. Successful collision-avoiding with scenario a), scenario b), scenario c).

TABLE 1. Successful lane-changing for 3 scenarios.

Scen.	Item	V1	V2	V3	V4	VB
Scen. a)	Initial Vel (km/h)	120	120	120	120	100
	Initial Pos(m)	150	150	50	50	100
Scen. b)	Initial Vel (km/h)	60	60	60	60	40
	Initial Pos(m)	150	150	50	50	100
Scen. c)	Initial Vel (km/h)	30	30	30	30	20
	Initial Pos(m)	150	150	50	50	100

returning to the original lane. The unsuccessful lane-changing is due to the traffic flow vehicles in the target lane entering the safety corridor of vehicle VB, and vehicle VB returns to the original lane in order to avoid collision, as shown in Fig.10.

2) Comparing the maximum acceleration priority strategy and the minimum acceleration priority strategy, the displacement characteristics (shown as in Fig.11), the time domain characteristics (shown as in Fig.12), the acceleration characteristics (shown as in Fig.13), the velocity characteristics (shown as in Fig.14) of lane changing have little difference with the two acceleration priority strategies when changing

TABLE 2. Successful collision-avoiding for 3 scenarios.

Scen.	Item	V1	V2	V3	V4	VB
Scen. d)	Initial Vel (km/h)	120	120	120	120	100
	Initial Pos(m)	150	150	0	50	100
Scen. e)	Initial Vel (km/h)	60	60	60	60	40
	Initial Pos(m)	150	130	0	99	50
Scen. f)	Initial Vel (km/h)	30	30	30	30	20
	Initial Pos(m)	150	135	50	110	100

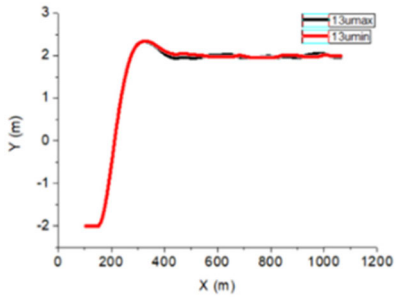

FIGURE 11. Displacement characteristics of lane-changing with 120km/h traffic flow.

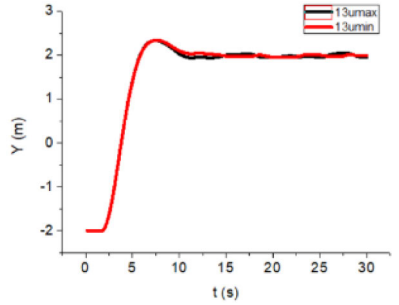

FIGURE 12. Time domain characteristics of lane-changing with 120km/h traffic flow.

lanes at an initial velocity of 100km/h in a traffic flow of 120km/h. The reason is that the high power dissipation such as wind drag of the vehicle at high velocity limits the variation range of longitudinal acceleration, and thus the variation value of longitudinal acceleration is small. It can be seen from Fig.13 that the variation range of a_x is merely $-0.31 m/s^2$ to $1.55 m/s^2$. This longitudinal acceleration is used to adjust the velocity of vehicle VB from 100km/h to the traffic flow velocity of 120km/h, and to adjust the longitudinal distance in the vicinity of its own lane and the target lane for collision avoidance. Under the constraint of safety corridor between vehicles, the initial condition that the average distance between vehicles at high velocity is merely 50m also further restricts the range of acceleration.

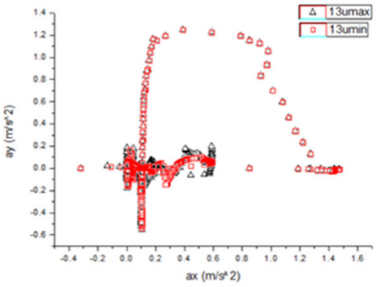

FIGURE 13. Acceleration characteristics of lane-changing with 120km/h traffic flow.

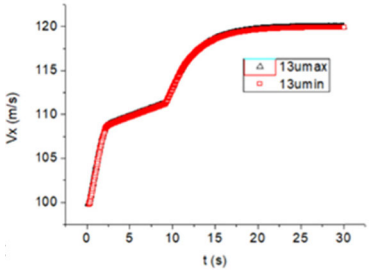

FIGURE 14. Velocity characteristics of lane-changing with 120km/h traffic flow.

TABLE 3. Forms of lateral acceleration (m/s^2).

Scen.	Item	$CEN_{a_y(k)}$	$RMS_{a_y(k)}$
High velocity (120km/h)	ax Maximized	0.16	0.25
	ax Minimized	0.17	0.25
Med. velocity (60km/h)	ax Maximized	0.20	0.23
	ax Minimized	0.19	0.24
Low velocity (30km/h)	ax Maximized	0.44	0.22
	ax Minimized	0.28	0.23

We mark the discrete form of centroid of lateral acceleration a_y as $CEN_{a_y(k)}$ in formula (27), and also mark the discrete form of root mean square of lateral acceleration a_y as $RMS_{a_y(k)}$, in formula (28). Two forms of lateral acceleration a_y, as shown in Table 3, can be obtained in different acceleration strategies with three typical vehicle velocities.

$$CEN_{a_y(k)} = \frac{\int a_y dA}{A} = \frac{\sum_{k=1}^{n} \{a_y(k) \left| a_y(k) \right| \}}{\sum_{k=1}^{n} \left| a_y(k) \right|} \tag{27}$$

$$RMS_{a_y(k)} = \sqrt{\frac{\sum_{k=1}^{n} \{(a_y(k))^2\}}{n}} \tag{28}$$

Analyzing the MPC optimized output data points, we can find out that the vehicle velocity V increases, $CEN_{a_y(k)}$ decreases, but $RMS_{a_y(k)}$ is almost unchanged, as shown in Table 3. This is due to the existence of many negative acceleration points with a_y at high vehicle velocities, and the acceleration distribution point diagram also confirms this inference, as shown in Fig.13. While v_x increases, $a_y = v_x^2/R$

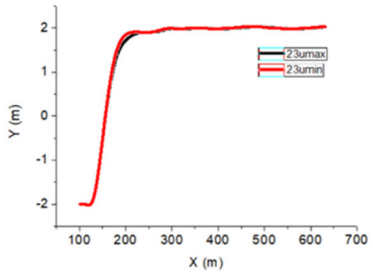

FIGURE 15. Displacement characteristics of lane-changing with 60km/h traffic flow.

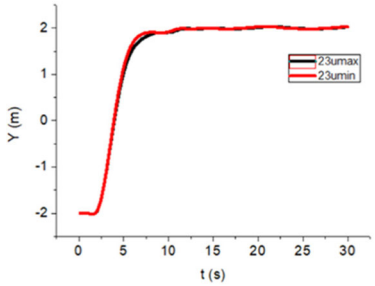

FIGURE 16. Time domain characteristics of lane-changing with 60km/h traffic flow.

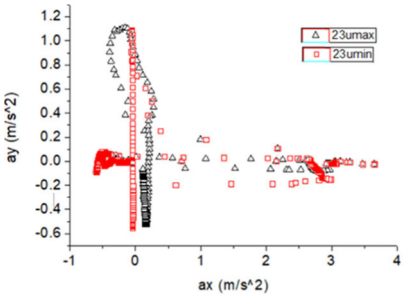

FIGURE 17. Acceleration characteristics of lane-changing with 60km/h traffic flow.

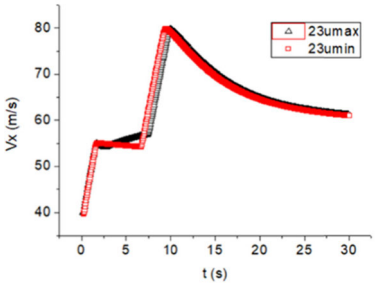

FIGURE 18. Velocity characteristics of lane-changing with 60km/h traffic flow.

also increases. There are 13 data points with lateral acceleration a_y greater than 1.0m/s^2 in the two acceleration priority strategy diagrams of lane changing. Since the resultant acceleration has a limited range, the a_x range must be reduced at high velocity to comply with the elliptical law of tire friction. It is worth noting that a_x includes the dissipative acceleration terms defined by Formula (18) in the two acceleration strategies. The following discussion is the same way as here.

Comparing the maximum acceleration priority strategy and the minimum acceleration priority strategy, the displacement characteristics (shown as in Fig.15), the time domain characteristics (shown as in Fig.16), the acceleration characteristics (shown as in Fig.17), the velocity characteristics (shown as in Fig.18) of lane changing have some differences with the two acceleration priority strategies when changing lanes at an initial velocity of 40km/h within a traffic flow of 60km/h.

Changing lanes with the maximum acceleration priority strategy, there is lane-changing time lag, lane-changing extension of the longitudinal distance, delay of lane-changing velocity, the range increase of longitudinal acceleration of lane-changing, and the increase of operating points of acceleration and braking, but the extent of those variations is not too great. The reason is that the dissipation power such as wind drag of vehicle VB is reduced when driving at a medium velocity, which relaxes the change range of longitudinal acceleration, and the variation of longitudinal acceleration increases. It can be seen from the Fig. 17 that the range of a_x varies from -0.7m/s^2 to 3.9m/s^2. This longitudinal acceleration is used to adjust the velocity of vehicle VB from 40km/h to the traffic flow velocity of 60km/h, and to adjust the longitudinal distance in the vicinity of its own lane and the target lane for collision avoidance. To the maximum acceleration priority lane changing strategy, the increase in the operating conditions of acceleration and braking will lead to a slight increase in lane changing time, shown as in Fig.16.

Comparing the maximum acceleration priority strategy and the minimum acceleration priority strategy, the displacement characteristics (shown as in Fig.19), the time domain characteristics (shown as in Fig.20), the acceleration characteristics (shown as in Fig.21), the velocity characteristics (shown as in Fig.22) of lane changing have large differences with the two acceleration priority strategies when changing lanes at an initial velocity of 20km/h within a traffic flow of 30km/h.

Changing lanes with the maximum acceleration priority strategy, there is lane-changing time lag, lane-changing extension of the longitudinal distance, delay of lane-changing velocity, the range increase of longitudinal acceleration of lane-changing, and the increase of operating points of acceleration and braking. These variations are much more apparent. The reason is that the dissipation power such as wind drag of the vehicle is very small when driving at low velocity, and the variation range of longitudinal acceleration increases significantly. It can be seen from Fig. 21 that a_x varies from -3m/s^2 to 6m/s^2. This longitudinal acceleration is used to adjust the initial velocity of the vehicle VB from 20km/h to 30km/h of the traffic flow, and to adjust the longitudinal distance in the vicinity of its own lane and the target lane for collision avoidance. When adjusting the distance between vehicles, the maximum velocity reaches as much as 52km/h, which is almost two times the velocity of the traffic flow. The three stages of lane change are composed of two simple

TABLE 4. List of notations.

SYMBOLS	EXPLANATIONS	UNITS
X, Y	Fixed plane coordinates in the ground frame	m
x, y	Fixed plane coordinates in the vehicle frame	m
φ	Heading angle	Rad
φ_{road}	Course angle	Rad
$\dot{e}_{\varphi}$	Derivative of the heading deviation	Rad/s
$\dot{e}_{d}$	Derivative of the lateral distance deviation	m/s
R	Curvature of the road	m
v_x, v_y	sub-velocities of the vehicle in X-Y coordinates	m/s
a_x, a_y	sub-accelerations of the vehicle in X-Y coordinates	m/s^2
b	Distance between the front axle and CG	m
c	Distance between the rear axle and CG	m
l	wheelbase of the vehicle	m
m	mass of the vehicle	kg
I_z	Moment of inertia of the vehicle	kg.m^2
r	Yaw rate	Rad/s
F_{xf},F_{yf}	Force of front tire with x or y direction in tire frame	N
F_{xr},F_{yr}	Force of rear tire with x or y direction in tire frame	N
α_f, α_r	Slip angle of front or rear tire	Rad
δ_f	Steering angle of the front wheel	Degree
$C_{\alpha f}$, $C_{\alpha r}$	Slip stiffness of front or rear tire	N/Rad
d,D,p	longitudinal travel distance of vehicle	m
ρ	Air density	kg/m^3
C_D	Aerodynamic drag coefficient	
A	Frontal area of the vehicle	m^2
Np	Total MPC control horizon	
N_s	Short MPC control horizon	
N_l	Long MPC control horizon	
T	Sampling period	s
T_s	Shorter time interval	s
T_l	Longer time interval	s
k_{sur}	Road surface coefficient	
μ	Peak coefficient of friction	
η	Shape factor	
λ	Summation weighting factor	
u	Manipulated variable or input variable	
Q(k)	Weighting matrix of state vector	
R(k)	Weighting matrix of input variable	
T(k)	Slack variables matrix of vehicle state	
W(k)	Slack variables matrix of path error	

longitudinal control stages and one longitudinal-lateral joint control stage. It can be seen that when the difference between the vehicle velocity and the velocity of the traffic flow is not large in the low-velocity traffic flow, using the maximum acceleration strategy to change lanes will otherwise make the lane changing slower.

While changing lanes at low velocity, following the maximum acceleration strategy control will cause large fluctuations in vehicle velocity. Although the time required for the longitudinal-transverse joint control is reduced, the time for the two simple longitudinal control phases will increase in case of great velocity fluctuation. The result is that under this low- velocity operating condition, according to the maximum acceleration priority strategy, the acceleration and braking operating conditions increase, the lane change time increases by about 9 seconds, and the lane change distance increases by over 20 meters.

We can find out that $CEN_{a_y(k)}$ increases in the low vehicle velocity of 30km/h, but $RMS_{a_y(k)}$ is almost unchanged, as shown in Table 3. This is due to the fact that a_y has many positive acceleration points at low vehicle velocities with the

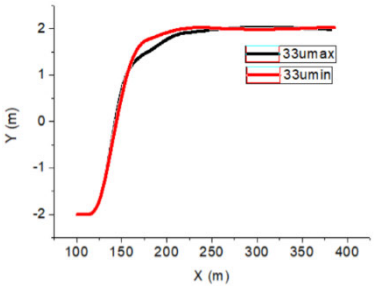

FIGURE 19. Displacement characteristics of lane-changing with 30km/h traffic flow.

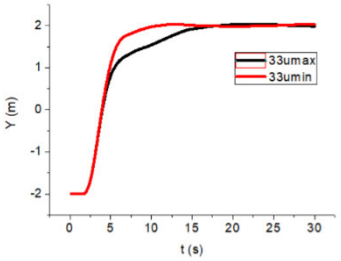

FIGURE 20. Time domain characteristics of lane-changing with 30km/h traffic flow.

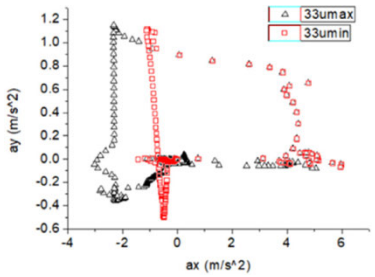

FIGURE 21. Acceleration characteristics of lane-changing with 30km/h traffic flow.

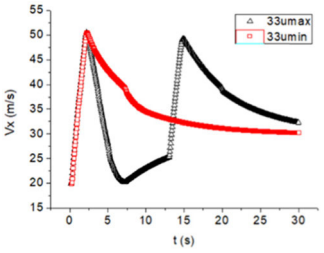

FIGURE 22. Velocity characteristics of lane-changing with 30km/h traffic flow.

maximum acceleration strategy. The acceleration distribution point diagram also confirms this result, shown in Fig. 21. While v_x decreases, $a_y = v_x^2/R$ is also down. There are only 8 data points with lateral acceleration greater than 1.0m/s^2 in either acceleration priority lane changing strategy diagram. Since the resultant acceleration has a limited range, the a_x range can be increased at low velocity and the tire force will not tend to be saturated.

All of the notations in this paper are given out with Table 4, which includes the symbols, its explanations and its units.

VI. CONCLUSION

1) The state equations of the vehicle dynamics model of the path tracking dynamic variables and tracking errors are established, and the weighting optimization of the state variable vector and the control variable increment is used to realize the MPC optimization control of the autonomous vehicle path planning. Further, the front steering wheels are indirectly controlled by adjusting the lateral force of the front wheels. In order to improve the accuracy of the model, the coefficient matrices of the discrete state equation perform an iterative optimization calculation as constant ones in the prediction horizon of this sampling time, and the next sampling time is treated as variable ones. Through MPC optimization with soft constraints, vehicles can break through the constraints of control accuracy and achieve obstacle avoidance.

2) The longitudinal and lateral control logics of the autonomous vehicle in the safety corridor of the traffic flow within the prediction horizon are analyzed, and the influences of the minimum longitudinal acceleration priority strategy on the lane changing characteristics at different vehicle velocities are compared, including overshoot oscillation, underdamping, hysteresis, and also the scene of unsuccessful lane-changing.

3) Considering three typical vehicle velocities, the influences of the maximum longitudinal acceleration priority strategy and the minimum longitudinal acceleration priority strategy on the displacement, velocity and acceleration of the lane changing are simulated, and the causes of lag of the lane changing are analyzed from the perspective that the tire longitudinal and lateral forces are constrained by the tire friction circle. When the velocity of the self-driving vehicle is much near to the velocity of the traffic flow, it is possible to complete the lane changing as soon as possible by adopting the minimum longitudinal acceleration priority strategy.

Future work will center on verifying the effectiveness of the proposed control algorithm and the real-time performance of MPC control on real roads.

REFERENCES

[1] B. Paden, M. Cap, S. Z. Yong, D. Yershov, and E. Frazzoli, "A survey of motion planning and control techniques for self-driving urban vehicles," *IEEE Trans. Intell. Vehicles*, vol. 1, no. 1, pp. 33–55, Mar. 2016.

[2] M. Cunningham and M. A. Regan, "Autonomous vehicles: Human factors issues and future research," in *Proc. Australas. Road Saf. Conf.*, 2015, pp. 1–11.

[3] S. A. Bagloee, M. Tavana, M. Asadi, and T. Oliver, "Autonomous vehicles: Challenges, opportunities, and future implications for transportation policies," *J. Modern Transp.*, vol. 24, no. 4, pp. 284–303, Dec. 2016.

[4] F. A. Mullakkal-Babu, M. Wang, B. van Arem, and R. Happee, "Empirics and models of fragmented lane changes," *IEEE Open J. Intell. Transp. Syst.*, vol. 1, pp. 187–200, 2020.

[5] F. Molinari, A. Grapentin, A. Charalampidis, and J. Raisch, "Automating lane changes and collision avoidance on highways via distributed agreement," *At-Automatisierungstechnik*, vol. 67, no. 12, pp. 1047–1057, Nov. 2019.

[6] J. Funke, M. Brown, S. M. Erlien, and J. C. Gerdes, "Prioritizing collision avoidance and vehicle stabilization for autonomous vehicles," in *Proc. IEEE Intell. Vehicles Symp. (IV)*, Jun. 2015, pp. 1134–1139.

[7] A. N. Spielberg, M. Brown, R. N. Kapania, C. J. Kegelman, and J. C. Gerdes, "Neural network vehicle models for high-performance automated driving," *Sci. Robot.*, vol. 4, no. 28, pp. 1–13, 2019.

[8] J. K. Subosits and J. C. Gerdes, "From the racetrack to the road: Real-time trajectory replanning for autonomous driving," *IEEE Trans. Intell. Vehicles*, vol. 4, no. 2, pp. 309–320, Jun. 2019.

[9] J. M. Maciejowski, *Predictive Control With Constraints*, Upper Saddle River, NJ, USA: Prentice-Hall, 2000.

[10] L. Wang, *Model Predictive Control System Design and Implementation Using MATLAB*, New York, NY, USA: Springer-Verlag, 2009.

[11] J. Liu, P. Jayakumar, L. J. Stein, and T. Ersal, "Combined speed and steering control in high-speed autonomous ground vehicles for obstacle avoidance using model predictive control," *IEEE Trans. Veh. Technol.*, vol. 66, no. 10, pp. 8746–8763, Oct. 2017.

[12] M. Ren, G. Wu, X. Chen, and X. Liu, "Model predictive automatic lane change control for intelligent vehicles," SAE, Warrendale, PA, USA, Tech. Rep. 2020-01-5025.

[13] P. Falcone, F. Borrelli, H. E. Tseng, J. Asgari, and D. Hrovat, "Linear time-varying model predictive control and its application to active steering systems: Stability analysis and experimental validation," *Int. J. Robust Nonlinear Control*, vol. 18, no. 8, pp. 862–875, May 2008.

[14] V. Turri, A. Carvalho, H. E. Tseng, K. H. Johansson, and F. Borrelli, "Linear model predictive control for lane keeping and obstacle avoidance on low curvature roads," in *Proc. 16th Int. IEEE Conf. Intell. Transp. Syst. (ITSC)*, Oct. 2013, pp. 378–383.

[15] K. Liu, J. Gong, A. Kurt, H. Chen, and U. Ozguner, "Dynamic modeling and control of high-speed automated vehicles for lane change maneuver," *IEEE Trans. Intell. Vehicles*, vol. 3, no. 3, pp. 329–339, Sep. 2018.

[16] D. G. Thomas, *Fundamentals of Vehicle Dynamics*. Warrendale, PA, USA: Society of Automotive Engineers, 1992.

FUZHOU ZHAO received the B.S. degree from the School of Automobile Engineering, Wuhan University of Technology, China, in 1998, the M.S. degree from the College of Energy and Power Engineering, Nanjing University of Aeronautics and Astronautics, China, in 2006, and the Ph.D. degree from the School of Mechanical Engineering, Nanjing University of Science and Technology, China, in 2010.

He is currently an Associate Professor with Changshu Institute of Technology. His research interests include vehicle dynamics modeling, path planning, and controlling for autonomous vehicles.

WENYE WU received the B.S. degree in mechanical design, manufacturing, and automation from Sanjiang University, Nanjing, China, in 2012, and the M.S. and Ph.D. degrees in agricultural mechanization engineering and power electronics and power transmission from Jiangsu University, Jiangsu, China, in 2015 and 2019, respectively.

He is currently a Lecturer with the School of Automotive Engineering, Changshu Institute of Technology. His research interests include design and optimization of permanent magnet machines for application in electric vehicles.

YANG WU received the B.S. degree from the School of Mechanical Engineering, Southwest Jiaotong University, China, in 2000, the M.S. degree from the National Key Research Center for Traction Power, Southwest Jiaotong University, China, in 2004, and the Ph.D. degree from the School of Traffic and Transportation, Southwest Jiaotong University, in 2009.

He is currently a Lecturer with Changshu Institute of Technology. His research interests include intelligent transportation systems and path/motion planning for automated driving.

QINGZHANG CHEN received the B.S. degree from the College of Engineering, Jiangxi Agricultural University, Jiangxi, China, in 1998, the M.S. degree from the College of Engineering, South China Agricultural University, Guangdong, China, in 2005, and the Ph.D. degree from the School of Automotive and Traffic Engineering, Jiangsu University, Jiangsu, China, in 2008.

He is currently a Professor with Changshu Institute of Technology. His research interests include vehicle dynamics and distributed driving system controlling.

YIQUAN SUN received the B.S. and M.S. degrees in mechanical engineering from the Armored Force Engineering Institute, Beijing, China, in 2007, and the Ph.D. degree in vehicle engineering from the Armament Engineering Institute, Shijiazhuang, China, in 2013.

He is currently a Researcher and a Faculty Member with Changshu Institute of Technology. He is the author of two technical books and over ten journal articles and conference papers. His current research interests include energy recovery and vibration controllability of vehicle chassis based on regenerative electromechanical suspension systems.

JIANWEI GONG received the B.S. degree from the National University of Defense Technology, Changsha, China, in 1992, and the Ph.D. degree from the Beijing Institute of Technology (BIT), Beijing, China, in 2002.

He was a Visiting Researcher with the Robotic Mobility Group, Massachusetts Institute of Technology, from 2011 to 2012. He is currently a Professor and the Director of the Intelligent Vehicle Research Center, School of Mechanical Engineering, BIT. His research interests include intelligent vehicle environment perception and understanding, driver behavior, and motion planning and control.